# SANDIA REPORT

SAND2012-5808
Unlimited Release
Printed August 2012

# NEAMS VLTS Project: Level 2 Milestone Summary

Glen A. Hansen, Jake T. Ostien, Qiushi Chen

Prepared by
Sandia National Laboratories
Albuquerque, New Mexico 87185 and Livermore, California 94550

Sandia National Laboratories is a multi-program laboratory managed and operated by Sandia Corporation, a wholly owned subsidiary of Lockheed Martin Corporation, for the U.S. Department of Energy's National Nuclear Security Administration under contract DE-AC04-94AL85000.



Sandia National Laboratories

Issued by Sandia National Laboratories, operated for the United States Department of Energy by Sandia Corporation.



Available to DOE and DOE contractors from
U.S. Department of Energy
Office of Scientific and Technical Information
P.O. Box 62
Oak Ridge, TN 37831

Telephone: (865) 576-8401
Facsimile: (865) 576-5728
E-Mail: reports@adonis.osti.gov
Online ordering: http://www.osti.gov/bridge

Available to the public from
U.S. Department of Commerce
National Technical Information Service
5285 Port Royal Rd
Springfield, VA 22161

Telephone: (800) 553-6847
Facsimile: (703) 605-6900
E-Mail: orders@ntis.fedworld.gov
Online ordering: http://www.ntis.gov/help/ordermethods.asp?loc=7-4-0#online

SAND2012-5808
Unlimited Release
Printed August 2012

# NEAMS VLTS Project: Level 2 Milestone Summary

Glen A. Hansen  Jake T. Ostien  Qiushi Chen

Sandia National Laboratories
P.O. Box 5800
Albuquerque, NM 87185-1321
gahanse@sandia.gov

**Abstract**

The objective of the U.S. Department of Energy Office of Nuclear Energy Advanced Modeling and Simulation (NEAMS) Very Long Term Storage (VLTS) Project is to develop a simple, benchmark model that describes the performance of Zry4 $\delta$-hydrides in cladding, under conditions of long-term storage of used fuel.

This model will be used to further explore the requirements of hydride modeling for used fuel storage and transport. It is expected that this model will be further developed as its weaknesses are understood, and as a basis of comparison as the Used Fuel Disposition (UFD) Campaign explores more comprehensive, multiscale approaches. Cladding hydride processes, a thermal model, a hydride model API, and the initial implementation of the J2Fiber hydride model is documented in this report.

# Contents



# Figures



# Tables

# 1 Introduction

The NEAMS Very Long Term Storage (VLTS) project focuses on the design and development of a fuel cladding hydride model to support cladding response calculations during extended storage and subsequent transport and handling operations. This scope of work was funded at $350K during FY2012. This document provides background on various concerns pertinent to modeling Zry4 $\delta$-hydride behavior in used fuel cladding and summarizes the progress of the NEAMS Very Long Term Storage (VLTS) project to date (06/29/2012) and the completion of the project level 2 milestone as described in the PICSNE project plan.

## 1.1 Background

There are several processes that potentially impact the long term storage and transport of used nuclear fuel. Cladding damage can occur throughout the life of the fuel; this damage can affect the retrieval of the fuel assemblies from the storage and transport casks, and can impact the ability of the cladding to contain its inventory during a transportation event. As discussed in the EPRI summary [**?**], the formation of radial hydrides during drying and storage may be one of the most important process to consider. However, it is important to note that the summary focuses on high burnup fuel given typical storage periods. The relative priorities of processes of potential concern may change for storage periods of 100-300 years. Further, as it is not possible to experimentally examine fuel under long term storage conditions, computational modeling and investigation of potentially impactful processes may be uniquely suited to this task. Given our current understanding of processes that weaken cladding during the drying and storage period, one of the more important is the presence of radial hydrides in the cladding.

During reactor operation, water coolant is in continual contact with the Zircaloy (Zry4) fuel cladding under elevated temperatures and pressures in a pressurized water reactor (PWR). A very small amount of water decomposes, the oxygen attacks the outsize surface of the Zry4 to form an oxide layer, typically less than 100$\mu$m thick (*c.f.* fig. 2-2 in [**?**]). Some of the hydrogen goes into solid solution within the Zry4, the amount of which depends on the Zry4 temperature and the diffusion rate. There is often a gradient in the amount of hydrogen in solution, the amount typically decreases with distance from the coolant. Thus, the amount of hydrogen contained in Zry4 is typically discussed in terms of maximum wall thickness average (MWTA) values that tend to increase with burnup (*c.f.* fig. 2-3 in [**?**]).

The solubility of hydrogen in Zry4 increases with temperature [**?**]. Discharged high burnup cladding can contain up to 800ppm hydrogen that is precipitated as circumferentially oriented hydride platelets located in a rim near the outer surface of the fuel (examined at room-temperature). During drying processes (around 400 C), there is roughly 200ppm of hydrogen in solution in the Zry4 that is available for precipitation as radial hydride given an appropriate hoop stress. The cooling strategy following the peak drying temperature appears to strongly affect the formation of radial hydride. Hong and Lee [**?**] show that holding an applied hoop stress load at 300 C for 7 hours prior to cooling promoted extensive formation of radial hydride.

One of the most comprehensive studies on the effect of cladding hydrides and their impact on used fuel transportation is summarized in an Electric Power Research Institute (EPRI) synthesis report ([**?**] and references contained therein). This report discusses and presents results from a damage-based three phase metal/hydride mixture model [**?**]. This model is subsequently improved in [**?**] to incorporate damage as a constitutive property.

This NEAMS project proposes to demonstrate an initial ability to study damage mechanics due to hydriding processes on domains similar to fig. 1, using a macroscale hydride damage model to estimate damage occurring during fuel drying and storage. As such, assessing cladding behavior during handling processes likely requires the ability to calculate the transient temperature of the fuel (recreate a correlation like (1)), calculation of the stress and strain in the cladding, and the calculation of the hydride induced damage given the transient conditions present during the fuel storage period.

## 1.2 VLTS Project Summary

One goal of this VLTS project is to develop and demonstrate a modeling capability comparable to that employed in the above EPRI studies. Toward this end, a significant portion of this project focused on understanding the details of the above work and developing modeling tools that could be employed in similar analysis scenarios. A technical workshop on modeling the mechanical effects of hydride reorientation during extended fuel storage was held Feb. 1, 2012 at Sandia National Laboratories in Albuquerque, NM. The four goals of the meeting were to:

- Define a basic initial hydride model to be implemented in a cladding response code
- Specify a simple validation process/problem (and data) to assess and compare to this model
- Identify the uncertainties in the input data and in the implementation of the model
- Define a proof-of-principle system response calculation that could be performed by October 2012

Requirements and strategies developed at this meeting were condensed into two documents for use in developing a functional application programming interface (API). Meeting notes [**?**] on the topics discussed during the meeting, including issues identified and suggestions about how to address them, were created. A second document [**?**] contains the strategy for developing a hydride reorientation model and the requirements that such a model should address. These documents were circulated to the attendees and edited based on their feedback.

The prototype hydride API, consisting of three prototype interfaces and tests that exercise them, was completed on March 30, 2012. The HydStress interface calls a MATPRO subroutine to calculate cladding stress. A second, more general interface supporting Sandia's LAME material model library was developed and tested in the event that the hydride model can be supplied as part of LAME. A third J2Stress interface, which would be the model for the native implementation of the

ultimate hydride functionality if LAME was not available, was also tested. The code supporting this API was made available in the form of a "git repository" on the machine `latrobe.sandia.gov`, where K. Clarno and M. Baird of ORNL have repository access.

Project staff met with Joe and Mark Rashid, and Bob Dunham at ANATECH in May to discuss outstanding questions and various details of the EPRI hydride reorientation model and results that it generates. Project staff also attended the UFD workshops in Las Vegas in November 2011 and in May 2012.

The final version of the hydride mechanical model, the *$J_2$ Fiber Damage Model*, was completed on June 29, 2012. The code that implements the model is checked into the ALBANY LCM code repository at Sandia, and an ALBANY regression test problem was developed to exercise various features of the model. Further, a demonstration prototype in the form of a mock ring compression test was developed to illustrate the basic performance of the model. The results produced by this model on this calculation are discussed later in this report. Additionally, the complete model was incorporated into the API library repository on `latrobe`.

Three areas of work remain to be performed on the model. First, project staff plan to function in an advisory role to ORNL AMP project staff as the model is integrated into AMP. The ALBANY ring compression test will serve as a benchmark to guide the AMP implementation and as a basis of comparison to verify that the implementation is correct. Secondly, work remains on calibrating the model to the correct $\delta$-hydride and Zry4 matrix material behavior under the environment of the ring compression tests to be performed. Lastly, the model needs to be modified to calculate hydride orientation based on local coordinates instead of global coordinates.

For the remainder of the project and FY, staff will focus on the above activities. However, during the development of the model, the importance of the hydride morphology (the local orientation, volume fraction, and the nature of hydride interconnection) on the performance (and derivation) of the model became very clear. In parallel to the above activities, we plan to develop a basic multiscale morphology model that could provide limited orientation data to the $J_2$ Fiber model. This model will be described later in this report.

# 2 The Thermal Model

Figure 2-5 in [**?**] develops a curve that estimates a cooling rate for fuel under typical storage conditions,

$$T(K) = 517.48 + 155.52\exp(-0.0877t) - 0.6922575t. \quad (1)$$

Such curves are developed by considering a hypothetical fuel rod within a cask. Figure 1 shows a hypothetical computational domain with the fuel at the center (in blue), surrounded by the clad, which is then surrounded by the cask and internal cask environment. One may perform an idealized heat transfer calculation, where the thermal conductivity in the fuel and cladding is employed to determine the heat flux through these components. A source term is used to generate the decay heat in the fuel. Figure 5-1 in [**?**] shows a fit to the decay power (in Watts/Assembly) over a 30 year storage history. The cask, remainder of the assembly, and the inert gas surrounding the fuel rod is modeled using an effective heat conduction value over the homogenized materials. The outer boundary holds a fixed temperature boundary condition meant to be representative of the surroundings (40 C).

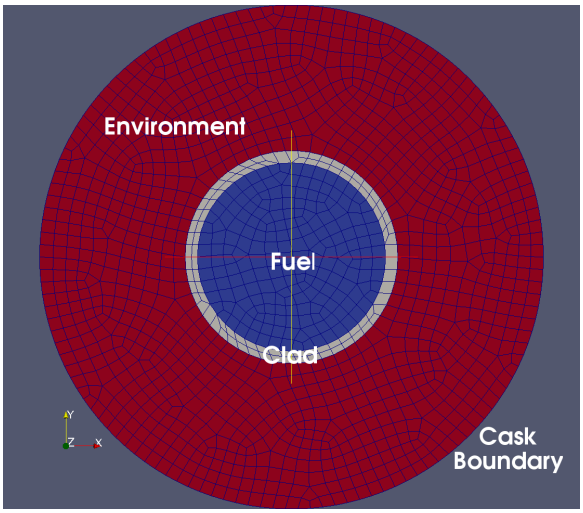


**Figure 1.** Cross-section of an idealized, homogenized fuel rod contained within an inert storage environment.

In this idealized analysis, the thermal conductivities of both irradiated fuel and cladding are well characterized. The effective conductivity of the environment in fig. 1 is not known. One may calculate a conservative overall conductivity value by noting that the fuel temperature is limited to 400 C during drying. Given the decay heat of the fuel, this maximum fuel temperature, the conductivities of the fuel and the clad, and the outside temperature of the cask, one may calculate an effective thermal conductivity for the environment such that the maximum fuel temperature is not exceeded during drying. Such an approach leads to fuel temperature curves similar to (1). Note that this approach would overpredict the fuel temperature during storage, as the storage cask environment after drying would transfer heat much more effectively than the partial vacuum present during drying.

**Figure 2.** Concentric cylindrical model with multiple regions of different thermal conductivity. Region 1 has conductivity $k_1$, radius $r_1$, internal heat generation term $\dot{q}$, and is made of $UO_2$.

This section describes the development of a homogenized thermal model to approximate the cladding temperature as a function of time over the drying and storage period. The homogenized result is in the form of a simple heat conduction problem, with a constant volumetric source in Region 1 (shown in fig. 2), that is surrounded by two different materials to form concentric cylinders. Region 1 is meant to be a reactor fuel that generates heat by radioactive decay at a constant rate $\dot{q}$. A ceramic material of moderate thermal conductivity $k_1$ and made of $UO_2$ fills the region. The radius is $r_1$, and the outside temperature of this area is $T_1$.

Zry4 metal, the fuel cladding, surrounds this fuel. The cladding has an outside radius $r_2$, a conductivity $k_2$, and an outside temperature $T_2$. Lastly, helium backfill (or vacuum) surrounds the cladding. The backfill region has a thermal conductivity $k_3$, radius $r_3$, and outside temperature $T_3$. The idea behind this test is to calculate the effective thermal conductivity $k_3$ of the helium/vacuum environment that surrounds the fuel/cladding while it is "dryed." Given a decay heat $\dot{q}$, what is the thermal conductivity of this material such that the peak internal temperature of the fuel (Region 1) does not exceed $400C$ given a surrounding environment temperature $T_3$ of $40C$?

Here, the concentric cylinders are modeled in two stages. The first stage uses a simplified form of (3.28) in [**?**]:

$$q_r = \frac{T_{\infty,1} - T_{\infty,4}}{\frac{1}{2\pi r_1 L h_1} + \frac{\ln(r_2/r_1)}{2\pi k_A L} + \frac{\ln(r_3/r_2)}{2\pi k_B L} + \frac{\ln(r_4/r_3)}{2\pi k_C L} + \frac{1}{2\pi r_4 L h_4}}. \tag{2}$$

For the problem described in fig. 2, and assuming that the length of the problem $L$ is unity, this becomes

$$q_r = \frac{T_1 - T_3}{\frac{\ln(r_2/r_1)}{2\pi k_2} + \frac{\ln(r_3/r_2)}{2\pi k_3}}. \tag{3}$$

Now, note that an overall energy balance at a radius of $r_1$ will give

$$q_r(r = r_1, \text{inside}) = q_r(r = r_1, \text{outside}), \tag{4}$$

or

$$\dot{q}(\pi r_1^2) = \frac{T_1 - T_3}{\frac{\ln(r_2/r_1)}{2\pi k_2} + \frac{\ln(r_3/r_2)}{2\pi k_3}}, \tag{5}$$

or

$$\frac{\dot{q} r_1^2}{2}\left[\frac{\ln(r_2/r_1)}{k_2} + \frac{\ln(r_3/r_2)}{k_3}\right] = T_1 - T_3, \tag{6}$$

or simply

$$\frac{\dot{q} r_1^2}{2}[\quad \cdot \quad] = T_1 - T_3. \tag{7}$$

Lastly, note that (3.52) in [**?**]

$$T(r) = \frac{\dot{q} r_o^2}{4k}\left(1 - \frac{r^2}{r_o^2}\right) + T_s, \tag{8}$$

may be rewritten for our case of the center cylinder $r_1$ as

$$T(r) = \frac{\dot{q}}{4k_1}\left(r_1^2 - r^2\right) + T_1. \tag{9}$$

As one is typically most interested in the temperature profile inside the fuel region 1, we can rewrite (7) in terms of $T_1$

$$T_1 = \frac{\dot{q} r_1^2}{2}[\quad \cdot \quad] + T_3 \tag{10}$$

and substitute this into (9) to yield

$$T(r) = \frac{\dot{q}}{4k_1}\left(r_1^2 - r^2\right) + \frac{\dot{q} r_1^2}{2}\left[\frac{\ln(r_2/r_1)}{k_2} + \frac{\ln(r_3/r_2)}{k_3}\right] + T_3. \tag{11}$$

To isolate $T_1$, we evaluate (11) at $r = r_1$,

$$T_1 = \frac{\dot{q} r_1^2}{2}\left[\frac{\ln(r_2/r_1)}{k_2} + \frac{\ln(r_3/r_2)}{k_3}\right] + T_3. \tag{12}$$

To isolate $T_2$, we note that $q_r$ in (4) is constant outside of the fuel $r \leq r_1$, so (5) can be written as:

$$\dot{q}(\pi r_1^2) = \frac{T_1 - T_3}{\frac{\ln(r_2/r_1)}{2\pi k_2} + \frac{\ln(r_3/r_2)}{2\pi k_3}} = \frac{T_2 - T_3}{\frac{\ln(r_3/r_2)}{2\pi k_3}}, \tag{13}$$

or

$$T_2 = \frac{\dot{q} r_1^2}{2}\left[\frac{\ln(r_3/r_2)}{k_3}\right] + T_3. \tag{14}$$

Now, we use (3.25) in [**?**], written appropriately, to calculate the temperature profile in the cladding $r_1 \leq r \leq r_2$,

$$T(r) = \frac{T_1 - T_2}{\ln(r_1/r_2)}\ln(\frac{r}{r_2}) + T_2, \tag{15}$$

and again for the cask environment $r_2 \leq r \leq r_3$,

$$T(r) = \frac{T_2 - T_3}{\ln(r_2/r_3)}\ln(\frac{r}{r_3}) + T_3. \tag{16}$$

## 2.1 Thermal Profile Results

The problem of interest concerns the fuel inside of a cannister inside a storage cask. First, it is necessary to determine the thermal conductivity of the "inert-ed" environment between the fuel rod and the cask, under the conditions of the drying/storage process. Known are the thermal conductivities of $UO_2$ and the cladding, and the decay heat in the fuel. Further, the ambient temperature on the outside of the cask is assumed, and the peak temperature in the fuel cannot exceed 400 C. This calculation will form the homogenized case.

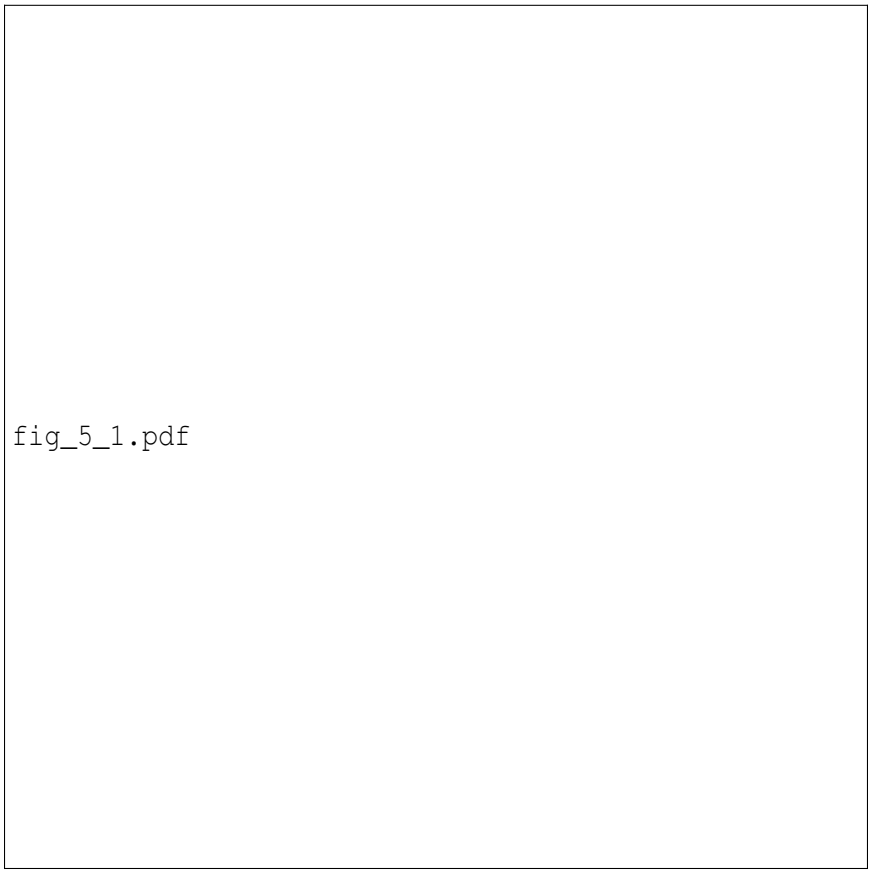


**Figure 3.** Decay heat from fission products under storage conditions, from [**?**].

Figure 3 is a recreation of fig. 5–1 in [**?**], that shows fuel decay heat history vs. time in years. This figure is used to create the heat source term in the test problem. Here, we assume there are 204 fuel rods per assembly and each rod is 149.7in in length [**?**]. We convert the units to W per unit length for the 2D test calculation as follows:

$$x\frac{\mathrm{W}}{\mathrm{Assy}} \times \frac{\mathrm{Assy}}{204\,\mathrm{rods}} \times \frac{\mathrm{rod}}{149.7\mathrm{in}} \times \frac{39.37\mathrm{in}}{\mathrm{m}} \tag{17}$$

**Table 1.** Material properties, constants, and dimensions used for the thermal calculation.

| Property | Value | Units | Source |
|---|---|---|---|
| $k(\mathrm{UO_2})$ | $k(T,x) = \lambda_0(T)\frac{\arctan(\theta(T,x))}{\theta(T,x)} + 5.95\times10^{-11}T^3$<br>$\lambda_0(T) = \left(3.24\times10^{-2} + 2.51\times10^{-4}T\right)^{-1}$<br>$\theta(T,x) = 3.67\exp\left(-4.73\times10^{-4}T\right)\sqrt{2x\lambda_0(T)}$ | $\mathrm{W\,m^{-1}\,K^{-1}}$ | [**?**] |
| $k$(clad) | $k(T) = 10.98 + 1.4\times10^{-2}T - 7.44\times10^{-6}T^2$ | $\mathrm{W\,m^{-1}\,K^{-1}}$ | [**?**] |
| $r(\mathrm{UO_2})$ | $r = 0.183$ | in | [**?**] |
| $r$(clad) | $r = 0.211$ | in | [**?**] |
| $l(\mathrm{UO_2})$ | $l = 0.6$ | in | [**?**] |
| $T$(max) | $T = 400$ | C | [**?**] |
| $r(\mathrm{UO_2})$ | $r_1 = 0.0046482$ | m | [**?**][1] |
| $r$(clad) | $r_2 = 0.0051562$ | m | [**?**][1] |
| $r$(cask) | $r_3 = 0.01$ | m | [2] |
| $l(\mathrm{UO_2})$ | $l = 0.01524$ | m | [**?**] |
| $T$(max) | $T = 673.15$ | K | [**?**] |
| $T_o$(ambient) | $T_o = 313.15$ | K | |
| $H_D(t(\mathrm{yr}))$ | $H_D = 273.986 + \frac{3113.11}{t^{0.6452}} + 9632.68\exp(-t)$ | W/Assy | [3] |
| $k(\mathrm{UO_2})$ | $k_1 = 4.9844$ | $\mathrm{W\,m^{-1}\,K^{-1}}$ | [4] |
| $k$(clad) | $k_2 = 17.033$ | $\mathrm{W\,m^{-1}\,K^{-1}}$ | [4] |

[1] We assumed that both the cladding ID and OD was smaller by the magnitude of the gap (0.008in [**?**]) or $r_1 = 0.183$in and $r_2 = 0.211 - 0.008 = 0.0203$in.

[2] This is not an important dimension for this calculation, thus an effective radius of 0.01m is used arbitrarily here.

[3] Curve fit to data given in fig. 5–1 in [**?**].

[4] Computed from formula in [**?**], assuming stoichiometric conditions $x = 0$ and maximum fuel temperature 673.15K.

Note that the "Best Fit Curve" shown in fig. 3 is drawn with the equation

$$\dot{q}(t) = 273.986 + 3113.11t^{-0.6452} + 9632.68\exp(-t), \tag{18}$$

where $t$ is in years and $\dot{q}$ is in units of Watts/Assembly.

The properties at the top of Table 1 are from [**?**]. To calculate the energy generation term, we use the curve fit to fig. 3, shown as $H_D$ in Table 1 to calculate the decay energy generation rate after 8.5 years of decay [**?**], in W/m. We use (17) for units conversion. This results in a source term of 1.364W/m at 8.5 years. Note that this is the heat generation in the fuel per meter of rod length. Multiplying by one meter (unit length) this gives the left hand side of (5), or

$$\dot{q}(\pi r_1^2) = 1.364\text{W}. \tag{19}$$

This approach assumes no temperature variation vertically in the rod. Given the radius of the $UO_2$ in the fuel, one may calculate the heat source term at 8.5 years to be

$$\dot{q} = 20095\text{W/m}^3. \tag{20}$$

**Figure 4.** Fuel temperature during storage.

**Figure 5.** Radial fuel temperature within the homogenized domain.

This process is repeated, given the appropriate decay heat value corresponding to each storage period, to create fig. 4. While a similar methodology was used to create it, fig. 4 differs from fig. 2-5 in [**?**] due to the consideration of the backfill conditions. Fig. 2-5 calculates an effective thermal conductivity in the cask at the peak of drying (when partial vacuum conditions exist), and assumes that this conductivity remains in effect throughout the storage period. Figure 4 attempts to approximate the effect of the helium backfill at the end of the dying phase with an increase in thermal conductivity of the cask environment. This adjustment lowers the fuel temperature to some extent after the drying phase. Note that it may be important to correctly capture the cooling rate during the backfill process, as hoop stresses predominate and it is thought that significant radial hydride formation may occur during this period [**?**].

Figure 5 shows an elevation plot of the radial fuel temperature in the idealized problem.

# 3 Overview of the EPRI Multiphase Mixture Model

The cladding model developed by EPRI [**?**, **?**] is a macroscale constitutive model based on the cladding being composed of volume fractions of four distinct components, base undamaged Zry4 metal, damaged (cracked) Zry4 metal, undamaged hydride platelet material, and damaged (cracked) hydride platelet material. The model is a two phase mixture model with the first phase ($\alpha = 1$) corresponding to the undamaged hydride platelets, and the second ($\alpha = 2$) undamaged Zry4 metal.

A notation similar to that described in [**?**] is employed here, where $\mathbf{e}_i$ $(i = 1,2,3)$ are the global coordinate system vectors and $\mathbf{e}'_i$ is a local coordinate system where $\mathbf{e}'_3$ is normal to the hydride platelet planes within the material. Note that the transformation between the global and local coordinate systems is typically different at each element integration point. One would select an idealized hydride platelet orientation valid at each integration point based on the surrounding conditions and history to develop the transformations between the coordinate systems. Note that in a given hydride morphology, there is a distribution in $\mathbf{e}'_3$ at a given integration point. Further, one would expect that the model would be sensitive to the assumed morphology; it would be quite interesting to study this sensitivity using UQ methods.

Let $\sigma^\alpha$ be the stress in each phase $\alpha$, and $D^\alpha$ be the rate of strain tensor

$$D = \frac{1}{2}\left(\nabla\mathbf{v} + (\nabla\mathbf{v})^T\right), \tag{21}$$

where $\nabla\mathbf{v}$ is the velocity gradient. The model first imposes that the normal strain rates in each of the two phases are equal in the plane of the hydride platelet, and they equal the normal strain rate of the aggregate, *i.e.,*

$$D'^1_{11} = D'^2_{11} = D'_{11} \tag{22}$$
$$D'^1_{22} = D'^2_{22} = D'_{22}. \tag{23}$$

Further, in the plane of the platelet, the shear strain rates of the phases match and equal the shear strain rate of the aggregate,

$$D'^1_{12} = D'^2_{12} = D'_{12}. \tag{24}$$

Next, one states that the shear stresses working on the platelet match and equal the shear stress of the aggregate,

$$\sigma'^1_{13} = \sigma'^2_{13} = \sigma'_{13} \tag{25}$$
$$\sigma'^1_{23} = \sigma'^2_{23} = \sigma'_{23}. \tag{26}$$

Finally, the normal stress to the platelets match,

$$\sigma'^1_{33} = \sigma'^2_{33} = \sigma'_{33}. \tag{27}$$

The hydride volume fraction is now used to complete the stress and strain rate tensors. Let $f$

be the volume fraction of the hydride platelet phase,

$$D'_{13} = fD'^{1}_{13} + (1-f)D'^{2}_{13} \tag{28}$$
$$D'_{23} = fD'^{1}_{23} + (1-f)D'^{2}_{23} \tag{29}$$
$$D'_{33} = fD'^{1}_{33} + (1-f)D'^{2}_{33}. \tag{30}$$

Similarly, the stress conditions are

$$\sigma'_{11} = f\sigma'^{1}_{11} + (1-f)\sigma'^{2}_{11} \tag{31}$$
$$\sigma'_{22} = f\sigma'^{1}_{22} + (1-f)\sigma'^{2}_{22} \tag{32}$$
$$\sigma'_{12} = f\sigma'^{1}_{12} + (1-f)\sigma'^{2}_{12}. \tag{33}$$

The next step of the model will be to develop the tangent moduli for the phases $\alpha$. Here, $C'^{\alpha}_{ijkl}$, where $ijkl$ each assume values from 1 to 3, are the elastic-plastic constitutive matrices for each phase $\alpha$. Given this definition, the stress-strain relationships of the phases are

$$\sigma'^{1}_{ij} = C'^{1}_{ijkl} D'^{1}_{kl} \tag{34}$$
$$\sigma'^{2}_{ij} = C'^{2}_{ijkl} D'^{2}_{kl} \tag{35}$$
$$\sigma'_{ij} = C'_{ijkl} D'_{kl} \tag{36}$$

The tangent moduli of the aggregate material is obtained from

$$C'_{ijkl} = fC'^{1}_{ijkl} + (1-f)C'^{2}_{ijkl}, \tag{37}$$

where in $C'^{\alpha}_{ijkl}$ each phase is $J_2$-elastic-plastic with a stress-strain curve described by

$$Y = Y_o \left[ 1 + \left( \frac{\varepsilon}{\varepsilon_o} \right)^n \right], \tag{38}$$

where $Y$ is the instantaneous yield stress, $Y_o$ is the initial yield stress, and $\varepsilon$ is the equivalent plastic strain. Here, $Y_o$, $\varepsilon_o$, and $n$ are specific to each phase, depending on the characteristics of each material. The properties of each platelet are a function of temperature only, and the properties of the base Zry4 matrix are a function of temperature and fluence, obtained from MATPRO [**?**].

The algorithm computing the above is from [**?**],

1. Set the maximum relative size of the strain-increment adjustment to be used.
2. Form a transformation matrix from the global coordinate system to the local system, at each integration point. To form the local system, one considers the hydride "layers", where the 3-direction is normal to the layers.
3. Choose which phase (1 or 2) will have its strain increment adjusted via iteration.
4. Set the convergence tolerance on the stress and set a reference strain-increment magnitude.

5. Form the components of the input strain increment with respect to the local integration point coordinate frame.

6. Set an initial estimate for the (stretching rate)*$\Delta t$ in each of the two phases, and form the final reference strain-increment magnitude.

7. Enter iteration loop to enforce equality between the two phases of tractions acting on the layers.

8. Evaluate the end-step stress and the tangent modulus for each of the two phases.

9. Adjust the strain increment for the phase and get components of the phase 1 and phase 2 modulus tensors given the layer coordinate frame.

10. Form the stress vector, and check it for convergence. If no convergence, then adjust the strain increment.

11. Scale the adjustment so that it is no bigger, in a norm, than the reference strain increment and form the adjusted strain increments for both phases.

12. Form the components of the adjusted strain increments in the global coordinate frame and close the iteration loop.

13. Set the updated state variables, form the composite stress, and form the composite tangent modulus.

14. Get the derivatives of the phase 1 and phase 2 strain increments with respect to the overall input strain increment.

15. Form the components of the composite tangent modulus with respect to the layer coordinate frame.

16. Set the components of the composite tangent modulus with respect to the global frame.

The damage model is described in [**?**]. If the above two phase model is subjected to stress high enough to damage the platelets (crack them), or the Zry4 metal, one will end up with a total of four domains. $\alpha = 1,2$ correspond to undamaged hydride platelets and base Zry4 metal as before. Now, $\alpha = 3,4$ correspond to damaged (cracked) platelet material and damaged Zry4 metal, respectively. The cracked material cannot support a traction in the $\mathbf{e}'_3$ direction, so for materials $\alpha = 3,4$,

$$D'^{\alpha}_{11} = D'_{11} \tag{39}$$
$$D'^{\alpha}_{22} = D'_{22} \tag{40}$$
$$D'^{\alpha}_{12} = D'_{12} \tag{41}$$
$$\sigma'^{\alpha}_{13} = \sigma'^{\alpha}_{23} = \sigma'^{\alpha}_{33} = 0. \tag{42}$$

The overall response is now given by the volume fraction expression,

$$\sigma' = \sum_{\alpha=1}^{4} f_\alpha \sigma'^{\alpha} \tag{43}$$

$$\mathbf{D}' = (f_1 + f_3)\mathbf{D}'^1 + (f_2 + f_4)\mathbf{D}'^2, \tag{44}$$

where $\sum_{\alpha=1}^{4} f_\alpha = 1$.

Damage (cracking) has occurred if either $f_3$ or $f_4 > 0$. The damage formulation to be employed is

$$\frac{f_3}{f_1 + f_3} = \frac{f_4}{f_2 + f_4} = g(e) \tag{45}$$

$$e(t) = \max_{\tau < t} \left[ \int_0^\tau D'^1_{33}\, d\tau \right], \tag{46}$$

*i.e.,* $e(t)$ is the maximum normal strain along $\mathbf{e}'_3$ observed thus far. The damage function is defined as

$$g(e) \equiv G(e, f; e_o, f_o) = \begin{cases} 0 & , \quad e \le \frac{e_o}{2} \\ \left( \frac{e - e_o/2}{\bar{e} - e_o/2} \right)^2 & , \quad \frac{e_o}{2} < e < \bar{e} \\ 1 & , \quad e \ge \bar{e} \end{cases} \tag{47}$$

with $\bar{e} = e_o(1 - f_o + f_o/\sqrt{f})$. Here, the material parameters are $e_o$ and $f_o$. The input data $E, K, n, m$ and $\dot{\varepsilon}_o$ are obtained from MATPRO and adjusted according to Section V.1 in [**?**]. Values for $f_o$ and $e_o$ are also from [**?**]. The behavior of the above model with the experimental and computed data given in figs. 6 and 7 of [**?**], are reproduced in fig. 6.

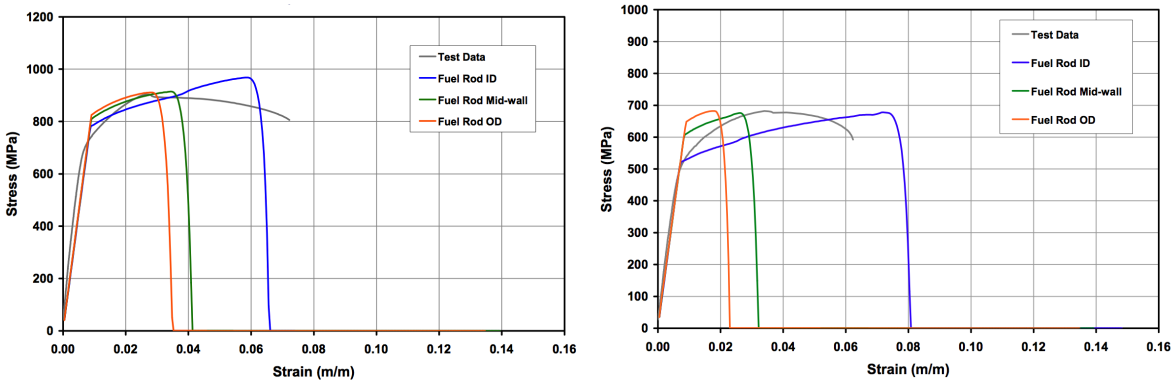


**(a)** Stress-strain response at 25 C.

**(b)** Stress-strain response at 300 C.

**Figure 6.** Stress-strain behavior of the model from [**?**].

# 4 Development of the Hydride Model API

The prototype hydride model API, consisting of three prototype interfaces and tests that exercise them, was completed on March 30, 2012. Three strategies and tests were included into the API and the tests that exercise it. The first was a basic link to the `cstress` subroutine in MATPRO [**?**]. In this case, a similar interface to the LAME library was constructed that evaluates both the residual and Jacobian contribution of the subroutine for use by applications that employ a Newton-like solver such at the ALBANY code. A simple unit test case was developed that exercises the MATPRO call; the results are shown in fig. 7.

**Figure 7.** MATPRO `cstress` calculation. Result generated by the API test case.

The second interface to be included in the API was a link to Sandia's LAME material library. This library is widely used; including the eventual hydride model into LAME allows re-use of both code inside LAME and allows convenient use of hydride data generated by the model by other applications. Currently, LAME is destined to become a template library that could be distributed outside Sandia. Unfortunately, this may not occur on a time frame to allow sharing of a hydride model inside of LAME with Oak Ridge National Laboratory on June 30, 2012.

As a fallback strategy and to support ready comparison, the $J_2$ Fiber model was included as an evaluator within the ALBANY code. The results of the model, as an ALBANY evaluator, follow in the next section.

# 5 The $J_2$ Fiber Damage Model

The $J_2$ fiber damage model is designed to model the mechanical response of the cladding material with hydrides oriented in multiple directions. The model treats the Zry4 matrix as a $J_2$ plastic material, and treats the hydrides as "fibers" that possess damage and that are oriented in particular directions (e.g., circumferential and radial directions). The stress response of the aggregate material is derived from a single stored strain-energy function, with contributions from both matrix and hydrides.

## 5.1 Model formulations

**Strain-energy function for cladding material with multiple preferred hydride directions**

A general form of the strain-energy function is hypothesized to have the following form:

$$\Psi = f_m(1-\xi_m)\Psi_m^0(C) + \sum_i^n f_i(1-\xi_i)\Psi_i^0(C,M), \tag{48}$$

where $C = F^T F$ is the right Cauchy-Green tensor. $M$ is the unit vector normal to the the hydride plane. $\Psi^0$ is the strain-energy function for undamaged material, $f$ is the volume fraction, and $\xi$ is the damage parameter. Subscripts '$m$' and '$i$' correspond to matrix and the $i^{\text{th}}$ hydride constituent, respectively. The volume fraction obeys the partition of unity property, *i.e.,*

$$f_m + \sum_i^n f_i = 1, \tag{49}$$

where $n$ is the number of hydride directions considered.

It is clear that the strain-energy function consists of contributions from both Zry4 matrix and hydrides. Damage parameters and volume fractions add flexibility to the model to capture a variety range of hydride compositions. The next step is to properly select strain-energy functions for different materials.

For the Zry4 matrix, we propose to use a $J_2$ type strain-energy function, commonly used for modeling elastoplastic behavior in metals, with isochoric plastic flow

$$\Psi_m^0 = U(J) + W(\bar{b}^e), \tag{50}$$

where

$$\begin{aligned} U(J) &= \frac{\kappa}{2}\left(\frac{1}{2}(J^2-1) - \log(J)\right) \\ W(\bar{b}^e) &= \frac{\mu}{2}(\mathrm{tr}(\bar{b}^e) - 3), \end{aligned} \tag{51}$$

and $\kappa$ and $\mu$ are the bulk and shear modulus, respectively.

The hydride component, on the other hand, endows the material with one or more preferred directions, which can be characterized by a unit vector $M_i$. If we define an invariant $I_{4(i)}$ for the $i^{\text{th}}$ hydride as

$$I_{4(i)} = M_i \cdot (CM_i), \tag{52}$$

and write the strain energy as a function of $C$ and $I_{4(i)}$. Then, the material properties will be independent of the sign choice of $M$, *i.e.,* $\Psi_i^0(C,M) = \Psi_i^0(C,-M)$. The strain-energy function still depends on $M$ but only through the invariant $I_{4(i)}$. One particular form of the strain-energy function, similar to those used to model fibers in composite materials, is used here

$$\Psi_i^0 = \frac{k_i}{q_i}\{\exp[q_i(I_{4(i)}-1)^2]\}, \tag{53}$$

with $k_i$ and $q_i$ being the two elastic constants for the $i^{\text{th}}$ hydride.

It should be emphasized that the specific energy functions proposed in this section are intended to capture some of the most salient features of the Zry4/hydride cladding materials. However, the strain-energy functions are by no means universal. With more available experimental data, different strain-energy functions may be used.

**Elastic constitutive law and stress**

With the strain-energy function proposed in (48), (50) and (53), it is straightforward to derive an elastic constitutive law and the stresses. For the $J_2$ matrix, the Kirchhoff stress tensor is obtained by the general expression

$$\tau^0 = 2F^e \frac{\partial \Psi_m^0}{\partial C^e} F^{e^T} = JU'(J)1 + s. \tag{54}$$

Substituting the energy form $\Psi_m^0$ for $J_2$, then the Kirchhoff stress tensor without damage can be expressed as

$$\begin{aligned} \tau^0 &= Jp1 + s \\ p = U'(J) &= \frac{\kappa}{2}(J - 1/J) \\ s &= \text{dev}(\tau) = \mu \text{dev}(\bar{b}^e). \end{aligned} \tag{55}$$

Then, considering damage, the Cauchy stress tensor for the matrix may be written as

$$\sigma_m = (1-\xi_m)\sigma^0 = (1-\xi_m)\tau^0/J. \tag{56}$$

For stress in fibers, the $2s^{\text{nd}}$ Piola-Kirchhoff stress tensor (without damage) is derived, resulting in

$$S_i^0 = 2\frac{\partial \Psi_i^0}{\partial C} = 4k_i(I_{4(i)}-1)\exp[q_i(I_{4(i)}-1)^2](M_i \otimes M_i). \tag{57}$$

Considering damage, the Cauchy stress tensor for the $i^{\text{th}}$ hydride can be written as

$$\sigma_i = (1-\xi_i)(F \cdot S_i^0 \cdot F)/J. \tag{58}$$

Following the uncoupled strain energy function in (48), the total Cauchy stress of the composite is the additive from the contributions from different components, *i.e.,*

$$\sigma = f_m \sigma_m + \sum_i^n f_i \sigma_i, \tag{59}$$

where $f_m$ and $f_i$ are the volume fractions for the matrix and $i^{\text{th}}$ hydrides, respectively.

#### Yield function and hardening law for the Zry4 matrix

The stress in the Zry4 matrix is restricted by the yielding condition, $F(\tau, \varepsilon^p) \leq 0$. Following [**?**], the yield surface may be written as

$$F(\tau, \alpha) = \|s\| - \sqrt{\frac{2}{3}}[Y_0 + H(\varepsilon^p)], \tag{60}$$

where $s = \text{dev}(\tau)$, and $Y_0$ is the initial yield strength, and $H(\alpha)$ is the hardening function that depends on the internal variable, *i.e.,* the equivalent plastic strain $\varepsilon^p$. A variety of forms of hardening functions can be selected; *e.g.,* linear, exponential, etc. One particular nonlinear hardening function can be written as

$$H(\varepsilon^p) = K\varepsilon^p + Y_\infty[1 - \exp(-\delta\varepsilon^p)], \tag{61}$$

where $K$ is the hardening modulus, $Y_\infty$ is the residual strength, and $\delta$ is the saturation exponent.

#### Damage evolution laws

For the damage variable $\xi$ appearing in the strain-energy function (48), a phenomenological smooth evolution law [**?**], is adopted

$$\xi(\alpha) = \xi_\infty[1 - \exp(-\alpha/\tau)], \tag{62}$$

where $\xi_\infty$ describes the dimensionless maximum damage and $\tau$ is referred to as the damage saturation parameter. $\alpha$ is identified in [**?**] as the maximum thermodynamic force.

## 5.2 Results of a ring compression test using the $J_2$ fiber damage model

Figure 8 is an idealization of a ring of Zry4 taking part in a ring compression test. Here, one-quarter symmetry applies, where the ring is compressed along the vertical direction by the test fixture. This compression results in a downward displacement of the top center of the ring, and an outward displacement of the right boundary of the ring, as seen exaggerated in the figure.

In the ring compression simulation, two hydride directions are considered. For simplicity, the first hydride direction is $\mathbf{M}_1 = [1,0,0]$, where the vector syntax $[x,y,z]$ denotes the coordinate

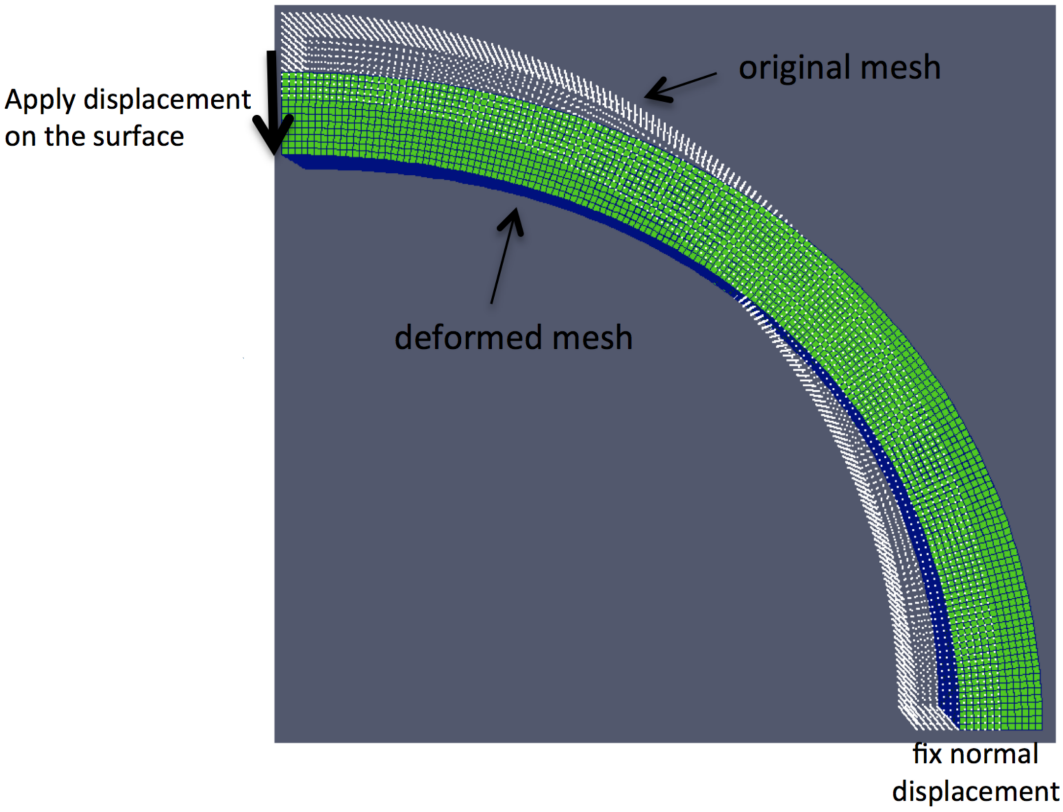


**Figure 8.** Ring of Zry4 in a hypothetical ring compression test. Symmetry is assumed to apply to allow analysis on one-quarter of the ring.

direction of the normal to the plane of the hydride platelet. Thus, the $\mathbf{M}_1$ hydride orientation is vertical and into the figure (the normal is along the $x$ axis. Similarly, the second hydride direction considered is the $\mathbf{M}_2 = [0,1,0]$ direction, with the hydride horizontal and into the figure. Work is underway to calculate hydride orientation based upon local coordinates instead of these fixed global coordinates. In this model, damage is active only in the hydride phases of the material.

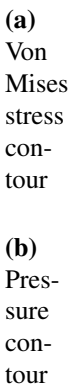


**Figure 9.** Stress contours in the ring test specimen.

These results are based on synthetic (uncalibrated) materials. The $J_2$ model employed for the matrix uses the properties $E = 206.9 \times 10^3$, $\nu = 0.29$, $\delta = 16.93$, $K = 129.24$, $\sigma_o = 450$, and $\sigma_\infty = 715$. The two hydride phases differ only in orientation $\mathbf{M}_1$ and $\mathbf{M}_2$, where $k_1 = k_2 = 1.0 \times 10^4$, $q_1 = q_2 = 1.0 \times 10^2$, $\xi_{\infty 1} = \xi_{\infty 2} = 1.0$, and $\tau_1 = \tau_2 = 100$. Properly calibrating the model to the Zry4 phases present is in process, as well as the direct comparison to ring compression test data such as the HB Robinson data being gathered by Argonne National Laboratory.

Figures 9(a) and 9(b) show the stress contours developed in the ring compression simulation. In fig. 9(a), it is clear that the Von Mises stress is concentrated where the load is applied along the center axis of the ring. The pressure field shows that the ring is in tension at the inner surface and in compression at the outer surface at the load application site. This stress concentration is consistent with the damage contours seen in figs. 10(a) and 10(b).

The damage contour illustrations are very interesting, in that the damage seen in the vertically-oriented $\mathbf{M}_1$ direction is of much higher magnitude that the horizontal hydride orientation. The scales of the two illustrations are identical; the damage encountered by the vertical hydride on the inner surface of the specimen under the load point is much greater than the damage seen elsewhere.

Figure 11 shows the load-displacement response of the ring specimen. It is clear that the volume fraction of hydride significantly influences the load carrying capacity of the ring. Further, the ability of the ring to resist loading is significantly reduced when hydride is present in comparison to the base $J_2$ model where the damage terms are inactive.

The model next requires calibration to the material properties of the base Zry4 matrix material and the $\delta$-hydride. Like the model described in section 3, MATPRO data could be used. Secondly,

**(a)** Von Mises stress contour

**(b)** Pressure contour

**Figure 10.** Stress contours in the ring test specimen.

**Figure 11.** Load vs. displacement behavior generated by the model on the ring compression simulation.

the model needs to be modified to calculate hydride orientation based on local coordinates instead of global coordinates, to allow focused study of the radial and circumferential directions in the ring compression specimen. This modification in underway within the ALBANY host code, but was not part of this study as the interface to the host code may be specific to each case.

The model in its current form requires hydride morphology information in addition to material properties. Prior to the use of the model, the user must isolate the hydride orientations of interest and estimate the volume fraction of hydride in each orientation. Such estimates are difficult to derive and are a major source of uncertainty and potential error in the model. This limitation of the modeling strategy presented here can be rectified with the development of a multiscale hydride morphology model as discussed in the next section.

# 6 Hydride Morphology Model

Both the evolution of the hydride morphology and the yield strength of the bulk cladding material are strongly affected by the stress and strain fields present in the cladding during drying, storage, and handling. One necessary precondition for the above $J_2$ Fiber model is the capability to estimate the local hydride morphology for input to the model, by coupling the temperature and stresses encountered during the drying phase. The project is developing a basic multiscale hydride morphology model that will significantly increase the fidelity and range of applicability of the tools that employ it, by directly linking the mesoscale $J_2$ model to a phase field hydride model at the mesoscale.

At the material grain scale, hydride inclusions form; the extent of which depends on the amount of hydrogen in the Zry4 matrix and the cooling rate/magnitude encountered during drying. The general orientation of these inclusions depend on the stress state during that cooling $\Delta T$ (the $\Delta T$ and bulk stress state can be calculated from a larger length scale simulation). There may also a stress-strain calculation to be performed at the mesoscale, as there will be a lower-length scale variation of stress magnitude and direction due to small scale effects that might affect the formation and orientation of these inclusions locally.

**Figure 12.** Couple macroscale temperature profile from RVE solution to parallel mesoscale morphology calculations.

The coupling of the meso and macroscale models will be done in two phases, the first of which is shown in fig. 12. In the first phase, the macro-scale will be decomposed into a set of representative volume elements (RVEs) that correspond to the different radial environments that exist within the cladding; (a) the hydrogen-rich region near the oxide layer, (b) the low hydrogen region near the fuel, and (c) the intermediate environment between these two. In this phase, we will pass the macroscale cladding temperature as a function of time and spatial location to a set of mesoscale calculations to compute the mesoscale hydride morphology during the drying and storage periods, as shown in fig. 13.

**Figure 13.** Coupled macroscale/mesoscale microstructural model.

The key advantage of the approach is to model the material evolution at the grain scale instead of exclusively relying on experimental data at the macroscale. Secondly, the multiscale model is less expensive that scaling up a lower-length scale model to be representative of the large scale geometry; we seek to leverage the relative strengths of the two simulation methods by coupling them in an automatic fashion.

Stage 2, shown in fig. 13, will add stress and strain coupling from the macro to the mesoscale, which is critical to predicting hydride formation and yield stress. Further, we will fully couple the transient meso-scale cladding strength and yield behavior back to the macro-scale calculation to

calculate aged fuel response under transport and handling conditions. Uncertainty quantification is being embedded in the framework to enable uncertainty propagation across the scales spanned by the model. Note that a similar multiscale linking concept has been demonstrated in a fuel performance application [**?**, **?**].

# 7 Summary

Staff attended the UFD Working Group Meeting held at UNLV May 15-17 and participated in several discussions concerning cladding mechanics and degradation during drying and long term storage and transport. Discussions were also held concerning possible follow-on work beyond the scope to be completed this FY. Staff also traveled to ANATECH in May and met with Joe and Mark Rashid, and Bob Dunham to discuss outstanding questions and various details of the EPRI hydride reorientation model and the results that it generates.

The milestone hydride mechanical model, the $J_2$ Fiber Damage Model, was completed on June 29, 2012. The code that implements the model is checked into the ALBANY code repository at Sandia, and a demonstration prototype consisting of a mock ring compression test was used to exercise the model. While the goal of the model was to demonstrate a basic, initial attempt at capturing the behavior of hydrided material, the results on this ring compression test geometry are encouraging. More detailed results of the model are presented in section 5. The model is also available as a component of the API repository on `latrobe.sandia.gov`.

The need to correctly estimate the hydride morphology of the material prior to loading is paramount with any material response model. Here, we propose a multiscale approach to compute this morphology during the drying phase of storage, and optionally during the storage period if warranted. The development of a multiscale model of this nature will be initiated this FY, but much of the scope of development and testing of this model will be in FY2013.

# DISTRIBUTION:

1 Kevin T. Clarno
Oak Ridge National Laboratory
P.O. Box 2008 MS6172
Oak Ridge, TN 37831-6172

2 John C. Wagner
Oak Ridge National Laboratory
P.O. Box 2008 MS6170
Oak Ridge, TN 37831-6170

3 Rob L. Howard
Oak Ridge National Laboratory
P.O. Box 2008 MS6170
Oak Ridge, TN 37831-6170

1 MS 1321 Randy Summers, 1443

1 MS 1321 Glen Hansen, 1443

1 MS 9042 Jake Ostien, 8256

1 MS 0747 Ken Sorenson, 6223

1 MS 0899 Technical Library, 9536 (electronic copy)

Sandia National Laboratories